VOL. 18, NO. 6, MARCH 2023 ISSN 1819-6608
ARPN Journal of Engineering and Applied Sciences

www.arpnjournals.com

FINITE ELEMENT ANALYSIS OF IRREGULAR POROUS SCAFFOLD FOR BONE TISSUE ENGINEERING

Rochmad Winarso[1,2], Rifky Ismail[3], P. W. Anggoro[4], J. Jamari[3] and A. P. Bayuseno[3]
[1]Department of Mechanical Engineering, Diponegoro University, Semarang, Indonesia
[2]Department of Mechanical Engineering, Faculty of Engineering, Universitas Muria Kudus, Indonesia
[3]Department of Mechanical Engineering, Faculty of Engineering, Diponegoro University, Indonesia
[4]Department of Industrial Engineering, Faculty of Industrial Technology, University of Atma Jaya Yogyakarta, Indonesia
E-Mail: rochmad.winarso@umk.ac.id

ABSTRACT

The structure of natural bone, particularly the trabecular structure, is irregular in the microscopic structure. Some related research had demonstrated that irregular porous structures like cancellous were better for cell growth. The correlations between irregular porous structure design parameters and porosity, average pore size, and associated mechanical properties are also complicated. This research uses finite element analysis to analyze irregular porous scaffold models of PLA/HA composite mechanical characteristics. The factors for the design parameters investigated in this study are strut diameters (SD), composite materials (M), and loading orientation (D). A full factorial design of experiments (FFD) was used to determine the optimal mechanical parameters of structure scaffold design. The results of our study illustrated that composite materials and strut diameter are essential factors for compressive strength and elastic modulus. Still, the strut diameter was the most critical variable in this simulation study. This study found that variation of loading direction at all irregular porous scaffolds in this research does little to affect compressive strength and elastic modulus. The optimization method showed that the desired results are obtained with the Z loading direction, 30% hydroxyapatite composition, and 0.65 mm strut diameter. Maximum compressive strength and elastic modulus were calculated to be 25.93 MPa and 1295.24 MPa, respectively. These results suggest that the bone scaffold elastic modulus and compressive strength are comparable to the trabecular bone but less than cortical bone.

Keywords: irregular porous scaffold, simulation analysis, full factorial design, hydroxyapatite, polylactic acid.

1. INTRODUCTION

Numerous factors, such as surface chemistry, roughness, pore size, pore interconnectivity, porosity, material chemical composition, and biocompatibility, were shown to influence the effectiveness of porous bone scaffolds [1]. Several porous scaffolds with linked pores have been produced in bone tissue engineering to attain excellent mechanical and biological properties. The capacity to adjust porosity, pore connectivity and strut diameter is critical in constructing a suitable scaffold [2]. Two requirements must be satisfied (1) The scaffold's exterior boundary surface must match the anatomy of the patient being replaced, and (2) the interior porous and interconnected structure of the scaffold must promote cell proliferation over the whole volume to be regenerated. As a result, the scaffold must replicate the geometry of the tissue transplant, and cell ingrowth necessitates a trabecular architecture with controllable porosity and pores size [3]. Porous structures are now divided into two types: regular porous structures and irregular porous structures [4]. The utilization of regular pores has been the base of most porous scaffold designs. Simple repletion of the unit cell or the triply periodic minimum surface is frequently used to create regular porous structures [4]. These regular structures include simple designs, predictable mechanical characteristics, and simple porosity control [5, 6].

The structure of natural bone, particularly the trabecular structure, is irregular in the microscopic structure [7]. The internal pore sizes and strut diameters of trabecular bone are not uniform, showing that the natural bone structure is irregular [8]. Some related research had demonstrated that irregular porous structures like cancellous were better for cell growth [9]. This fact showed that irregular porous structures are more suitable than regular structures. The mathematical modeling technique based on Voronoi-Tessellation achieves excellent results when developing approximations of natural irregular porous structures [10]. Deering *et al*. [11], Zhao *et al*. [12], and Fantini *et al*. [13]. have created a full-interconnected porous scaffold using a selective Voronoi tessellation approach. This approach has advantages such as trabecular-like structure and customizable design, and anisotropic porous scaffolds. They investigated the stability and impact resistance of regular porous structures, irregular porous structures, and gradient irregular porous structures based on Voronoi-tessellation. They concluded that Voronoi tessellation is an efficient strategy for creating three-dimensional porous scaffolds. The correlations between irregular porous structure design parameters and porosity, average pore size, and associated mechanical properties are also complicated [14]. Previous research has looked at the mechanical advantages of cellular Voronoi structures, where changes in the cellular structure isotropy may impact the structure's deformation mode and stiffness [11,15]There is a high correlation between the mechanical axis of the bone and trabecular orientation, where the direction of force transferred through the bone changes along the mechanical axis [16].

Polylactic acid is a synthetic polymer often utilized as a biomaterial in producing porous bone scaffolds. PLA is also recognized for developing bone

ARPN Journal of Engineering and Applied Sciences

scaffolds for their biocompatibility and controlled degradation rate after being introduced into the human body. Glassy PLA is inherently more brittle and rapidly degradable than PCL. Furthermore, it has less elasticity and flexibility. Blending with ductile polymers may increase the impact resistance and fracture toughness of the PLA [17].

Ceramics like hydroxyapatite (HA) have been combined with polymers to create composite biomaterials more functionally equivalent to the actual bone[18]. By adding bioactive phases like hydroxyapatite (HA) to polymer matrices, biocomposite materials are much more biocompatible and have higher mechanical properties [19]. Wu *et al*. [18] investigate the viability of PLA/HA composite printed models and evaluate morphological and mechanical characteristics. Gendviliene *et al*. [20] explore the morphological features of three-dimensional (3D) printed porous PLA and PLA/HAp scaffolds and the dimensional accuracy reliance on filament composition and FDM printer type. Mystiridou *et al*. [21] studied the use of 3D printing to create composite bioscaffolds that combine the bioactive characteristics of HA with a polymeric matrix composed of polylactic acid (PLA) and poly-caprolactone (PCL). Hassanajili *et al*. [19] investigate the potential of macro and micro porous PLA/PCL/HA scaffolds created by combining an indirect 3D printing technique with freeze-drying for bone tissue engineering. However, just a few reports on the mechanical characteristics and biocompatibility of PLA/HA trabecular-like scaffolds are based on Voronoi-Tessellation.

The production of bone scaffolds is one area of biomedical engineering research where simulation analysis has shown considerable promise [22, 23]. Simulation analysis is an alternate method for estimating mechanical properties concerning various scaffold design factors [24]. Zhang *et al.* [22] use the finite element method to figure out how the pore parameters affect the mechanical properties of the scaffolds before the scaffolds are made. Badge *et al*. [24] used finite element simulation to figure out how the effective modulus of different bioceramic composites would match up with the properties of cortical bone. This research uses finite element analysis to analyze irregular porous scaffold models of PLA/HA composite mechanical characteristics. This research is divided into three sections: (1) Investigate the effect of architecture design on scaffold porosity. (2) Finite element analysis of the scaffold with modified mechanical strength design parameters. (3) The relationship between porosity and effective Young's modulus for the best design architecture among the ones proposed.

2. MATERIALS AND METHODS

2.1 Material

The bone scaffold material in the simulation process is PLA and HA with material properties, as stated in Table-2.1.

Table-2.1. Properties of PLA and HA.

Materials	Chemical Composition	Elastic Modulus (MPa)	Poissons Ratio	Ref.
PLA	(C3H4O2)n	3500	0.36	[25]
HA	$Ca_{10}(PO_4)_6(OH)_2$	13000	0.27	[26]

The scaffold's material choice is a composite of hydroxyapatite (HA) and Polylactic acid (PLA). The chosen HA percentages are 5%, 10%, 15%, 20%, 25%, and 30%, with the remaining percentage being in reverse proportion. The Halpin-Tsai equation can be used to compute the mechanical characteristics of composite materials. The mechanical properties of the composite material can be estimated by Halpin-Tsai equation [24, 26, 27] shown in equations (1), (2), (3), and (4).

$$E_c = \frac{E_m(1+2s\times q\times V_p}{1-q\times V_p} \quad (1)$$

$$q = \frac{(\frac{E_p}{E_m}-1)}{(\frac{E_p}{E_m}+2s)} \quad (2)$$

$$\mu_c = \frac{\mu_m(1+2s\times q\times V_p}{1-q\times V_p} \quad (3)$$

$$q = \frac{(\frac{\mu_p}{\mu_m}-1)}{(\frac{\mu_p}{\mu_m}+2s)} \quad (4)$$

Where

E_c	: Elastic modulus of composite material	μ_c	: Poisson's ratio of composite material
E_m	: Elastic modulus of matric material	μ_m	: Poisson's ratio of matric material
E_p	:Elastic modulus of particle material	μ_p	:Poisson's ratio of particle material
s	: The aspect ratio of particle	Vp	: Volume of particle material

Table-2.2 presents the computed values for composite material.

ARPN Journal of Engineering and Applied Sciences

Table-2.2. The elastic modulus and Poisson's ratio of composite material.

Composite Material	Elastic Modulus (MPa)	Poisson's ratio
95%PLA/5%HA	3755	0.355
90%PLA/10%HA	4024	0.350
85%PLA/15%HA	4306	0.345
80%PLA/20%HA	4602	0.341
75%PLA/25%HA	4915	0.336
70%PLA/30%HA	5245	0.331

2.2 Method

The irregular scaffold is constructed so the various strut diameters can fit inside the four mm^3 cubes. CAD software developed the irregular structure scaffold design based on the strut's diameter. In bone scaffold design, porosity is an important property, defined as the volume ratio of pore space in a solid structure [28]. Porosity significantly impacts the mechanical strength and modulus elasticity of bone scaffolds. For optimal osseointegration, the porosity of the scaffold design should be larger than 50% [29]. The porosity of the irregular structure scaffold is determined by Equation (5) [26]. This study employs six irregular structure scaffolds with various strut diameters of 6.5, 6, 5.5, 5, 4.5, and 4 mm, as illustrated in Figure-2.1.

$$Porosity\ (\%) = 1 - \frac{V_{Solid}}{V_{Total}} \times 100\% \qquad (5)$$

Vsolid represents the solid volume scaffold, and Vtotal is its total volume. The solid volume scaffolds were calculated using CAD software to assess porosity. In order to examine the effects of strut diameter, composite materials, and loading directions on elastic modulus and compressive strength in irregular structure scaffolds, finite element simulations were performed. All irregular structure scaffolds CAD files were converted into Standard for the Exchange of Product model data (STEP) files and then simulated using Ansys Software. Finite element simulations use linear tetrahedral elements to discretize all of the samples. All materials in this investigation were modeled as homogeneous, isotropic, and linear elastic. Compression tests are conducted in three loading orientations, namely the X, Y, and Z axes. For the analysis, one side of the model was constrained by fixed support, while 0.08 mm (an equivalent strain of 2%) of displacement was applied to the opposite side facing, as illustrated in Figure-2.2. Displacement-controlled boundary conditions are used to execute numerical compression tests.

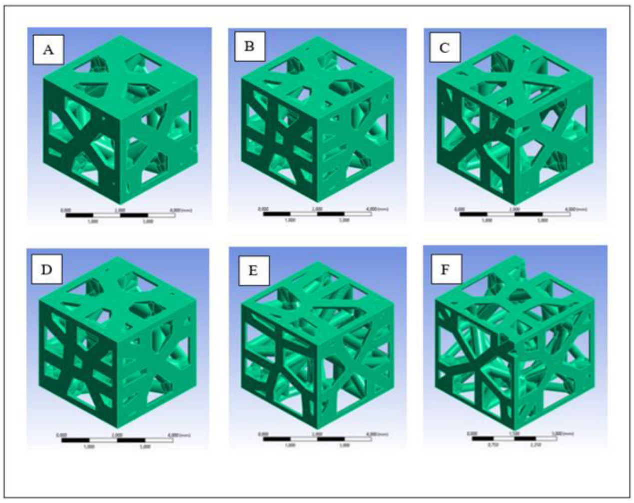

Figure-2.1. Design of irregular structure scaffold with strut diameter (A) 6.5 mm, (B) 6 mm, (C) 5.5 mm, (D) 5 mm, (E) 4.5 mm, and (F) 4 mm.

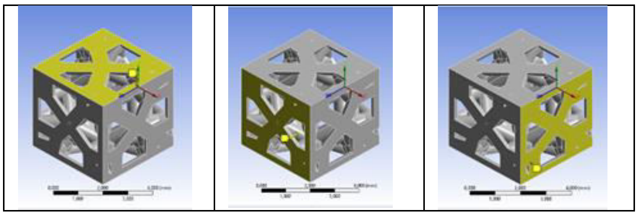

Figure-2.2. Loading orientation of irregular structure scaffold.

Mesh convergence is one of the essential factors in finite element analysis influencing accuracy. Mesh convergence establishes how many elements are necessary for a model to guarantee that altering the mesh size does not affect the outcomes of a study. To achieve mesh convergence, the simulation was conducted with varying element sizes with adaptive sizing mesh, 0.3 mm element size mesh, and 0.2 mm element size mesh. Table-2.3 displays the mesh convergence of force and stress in each simulation for the irregular structure in terms of the different element sizes. The percentage deviation in force and stress values must be less than 5% compared to the preceding element size [30].

Validation is required before receiving or approving the simulation findings. Validation in this work was accomplished by comparing simulation and analytic results. The analytical result of force and stress is calculated using Equations (5) to (7).

$$\Delta L = \frac{FL}{AE} \qquad (5)$$

$$\varepsilon = \frac{\Delta L}{L} \qquad (6)$$

$$\sigma = \frac{F}{A} \qquad (7)$$

Where ΔL is deformation in mm, F is the force in Newton, L is the original length in mm, A is the area in

mm^2, E is the elastic modulus in MPa, ε is the strain, and is the stress in MPa. The simulation data is generated by performing a sample compression test ten times with a displacement of 0.01, 0.02, and up to 0.1 mm. The variables compared in the simulation and analytic results were force vs. displacement. Figure-3 compares the mechanical characteristics of samples for both simulation and analytical data. Calculate porous scaffolds' maximal compressive strength by dividing the force at yield stress by the cross-sectional area [31].

Table-2.3. The mesh convergence of force and stress for each simulation.

Element Size	Nodes	Force (N)	Deviation(%)	Stress (MPa)	Deviation (%)
Adaptive sizing	41729	297.46		47.717	
0.3	44096	297.66	0.067	47.639	0.163
0.2	56876	296.49	0.326	46.669	2.196

2.3 Statistical Analysis

A full factorial design of experiments (FFD) was used to determine the optimal mechanical parameters of structure scaffold design. The most significant response data on factor main effects and interactions will come from a full factorial design of the experiment. Full factorials also allow factors to have a variable number of levels and will enable the process to be optimized once it has been validated.Table-2.4 shows the factors and their level for the design parameters investigated in this study.

Table-2.4. The specified variables' factors and their respective levels.

Factors	Level					
	1	2	3	4	5	6
Strut Diameters (SD)	0.4	0.45	0.5	0.55	0.6	0.65
HA Concentration (%) (M)	5	10	15	20	25	30
Loading Orientation (D)	Y	X	Z			

All quantitative data, including compressive strength and elastic modulus, were tabulated in the design matrix (Table-2.5.), followed by the necessary statistical analysis.

Table-2.5. Design matrix for full factorial design.

	Factors			Responds	
Run Order	D	M	SD	CS	EM
1	Y	5	0.4	6.38	311.43
2	Y	5	0.45	6.05	301.33
3	Y	5	0.5	7.95	391.14
4	Y	5	0.55	10.25	511.16
5	Y	5	0.6	16.70	833.29
6	Y	5	0.65	19.93	994.91
7	Y	10	0.4	6.84	333.57
8	Y	10	0.45	6.48	322.63
9	Y	10	0.5	8.51	418.85
10	Y	10	0.55	10.97	547.29
11	Y	10	0.6	17.88	892.28
12	Y	10	0.65	21.35	1065.51
13	Y	15	0.4	7.31	356.74
14	Y	15	0.45	6.93	344.99
15	Y	15	0.5	9.10	447.85
16	Y	15	0.55	11.73	585.16
17	Y	15	0.6	19.11	954.05
18	Y	15	0.65	22.83	1139.45
19	Y	20	0.4	7.81	381.07
20	Y	20	0.45	7.40	368.46
21	Y	20	0.5	9.72	478.32
22	Y	20	0.55	12.53	624.97
23	Y	20	0.6	20.42	1019.03
24	Y	20	0.65	24.38	1217.16
25	Y	25	0.4	8.34	406.77
26	Y	25	0.45	7.89	393.21
27	Y	25	0.5	10.38	510.49
28	Y	25	0.55	13.37	666.96
29	Y	25	0.6	21.79	1087.53
30	Y	25	0.65	26.03	1299.18
31	Y	30	0.4	8.89	433.87
32	Y	30	0.45	8.42	419.27
33	Y	30	0.5	11.06	544.34
34	Y	30	0.55	14.26	711.16
35	Y	30	0.6	23.23	1159.69
36	Y	30	0.65	27.76	1385.60
37	X	5	0.4	6.01	297.30
38	X	5	0.45	8.56	424.13
39	X	5	0.5	6.82	336.67

40	X	5	0.55	9.43	470.17
41	X	5	0.6	17.43	869.36
42	X	5	0.65	19.78	987.27
43	X	10	0.4	6.43	318.41
44	X	10	0.45	9.16	454.12
45	X	10	0.5	7.30	360.49
46	X	10	0.55	10.09	503.40
47	X	10	0.6	18.67	931.02
48	X	10	0.65	21.18	1057.30
49	X	15	0.4	6.88	340.53
50	X	15	0.45	9.80	485.56
51	X	15	0.5	7.81	385.43
52	X	15	0.55	10.79	538.25
53	X	15	0.6	19.96	995.60
54	X	15	0.65	22.65	1130.64
55	X	20	0.4	7.35	363.77
56	X	20	0.45	10.46	518.62
57	X	20	0.5	8.34	411.67
58	X	20	0.55	11.53	574.84
59	X	20	0.6	21.32	1063.50
60	X	20	0.65	24.20	1207.75
61	X	25	0.4	7.84	388.30
62	X	25	0.45	11.17	553.47
63	X	25	0.5	8.90	439.32
64	X	25	0.55	12.30	613.47
65	X	25	0.6	22.76	1135.13
66	X	25	0.65	25.83	1289.10
67	X	30	0.4	8.37	414.17
68	X	30	0.45	11.91	590.18
69	X	30	0.5	9.49	468.46
70	X	30	0.55	13.12	654.11
71	X	30	0.6	24.27	1210.63
72	X	30	0.65	27.55	1374.82
73	Z	5	0.4	6.53	325.72
74	Z	5	0.45	7.72	382.21
75	Z	5	0.5	7.43	369.40
76	Z	5	0.55	9.78	488.94
77	Z	5	0.6	17.04	852.19
78	Z	5	0.65	19.71	983.71
79	Z	10	0.4	6.99	348.85
80	Z	10	0.45	8.27	409.28
81	Z	10	0.5	7.95	395.52
82	Z	10	0.55	10.47	523.53
83	Z	10	0.6	18.25	912.56
84	Z	10	0.65	21.11	1053.47
85	Z	15	0.4	7.48	373.07
86	Z	15	0.45	8.84	437.65
87	Z	15	0.5	8.50	422.92
88	Z	15	0.55	11.20	559.78
89	Z	15	0.6	19.52	975.81
90	Z	15	0.65	22.57	1126.57
91	Z	20	0.4	7.99	398.53
92	Z	20	0.45	9.44	467.48
93	Z	20	0.5	9.08	451.68
94	Z	20	0.55	11.96	597.88
95	Z	20	0.6	20.85	1042.31
96	Z	20	0.65	24.11	1203.41
97	Z	25	0.4	8.53	425.41
98	Z	25	0.45	10.08	498.95
99	Z	25	0.5	9.69	482.03
100	Z	25	0.55	12.76	638.03
101	Z	25	0.6	22.25	1112.41
102	Z	25	0.65	25.73	1284.46
103	Z	30	0.4	9.10	453.71
104	Z	30	0.45	10.75	532.12
105	Z	30	0.5	10.33	514.02
106	Z	30	0.55	13.61	680.34
107	Z	30	0.6	23.73	1186.31
108	Z	30	0.65	27.44	1369.88

3. RESULTS AND DISCUSSIONS

3.1 Validation Process and Porosity of the Irregular Porous Structure

The sample's properties were analyzed through simulation and validated using an analytical method. Figure-3.1 compares the mechanical properties of PLA samples using simulation and analytical data. The simulation is executed using two types of meshing: adaptive meshing and 0.3 millimeter-sized elements. These results indicate that the difference between simulation and analytical results is statistically insignificant, with a relative error of less than 2%.

The cross-sectional area of the struts has a significant effect on the porosity of the irregular porous structure. The cross-section size and porosity for each sample are listed in Table-3.1. Based on these findings, all models have pore sizes consistent with those suggested by Mullen *et al.* [32]. Depending on the strut diameter of the scaffold, the porosity values were found to vary from 48 to

72 %. The porosity level should be as high as possible to get the best results. The more cavities in the scaffold, the more space there is for new tissue to grow [29]. The porosity was related to the design parameters: the struts' diameter and the unit cells' size. The findings indicate that the struts' diameter significantly affects the structure's porosity. A negative relationship between strut diameter and porosity is observed. Increasing the strut diameter of the scaffold structure results in less space inside the structure, reducing the scaffold's porosity.

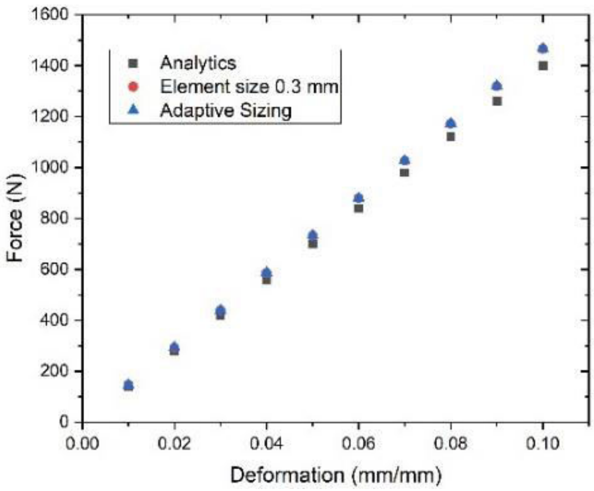

Figure-3.1. Validation diagrams of analytical and simulation method.

Table-3.1. The porosity of the irregular porous structure.

Unit Cell (mm)	Cross section size (mm)	Solid volume (mm^3)	Porous volume (mm^3)	Porosity (%)
4	0.65	64	33.153	48
4	0.6	64	30.553	52
4	0.55	64	26.375	59
4	0.5	64	23.023	64
4	0.45	64	20.896	67
4	0.4	64	17.611	72

3.2 Analysis of Variance (ANOVA)

Analysis of variance (ANOVA) provides the probability that the observed outcomes resulted from random chance. If a term's p-value is less than the significance level, the term will be statistically significant. The p-value was determined by dividing the adjusted mean square of the term by the adjusted mean square of the error to get the F-distribution value. The majority of researchers agree that the p-value must be equal to or lower than 0.05 for the operational variables to be statistically significant in influencing the examined response and for the null hypothesis for the ANOVA to be rejected [33, 34]. Table-3.2 and Table-3.3 show that composite material (M) and strut diameter (SD) are significant and have a confidence level of 100% in influencing compressive strength and elastic modulus since their p-value is zero, assuming that all seemingly small effects reflect the error. In contrast, a larger p-value for factor D (load direction) was insignificant.

Table-2.5. displays the results of calculating the compressive strength and elastic modulus of each item based on the recorded reaction force and measured dimensions using equation (7). Due to the fact that a single replicate of a full factorial design does not provide a direct error measure for ANOVA, normal probability plots (NPP) and Pareto plots of the effects are used to identify the larger, more likely significant effects.

Table-3.2. Analysis of variance (ANOVA) for compressive strength.

Source	DF	Adj SS	Adj MS	F-Value	P-Value
Model	12	4394.16	366.180	376.97	0.000
Linear	12	4394.16	366.180	376.97	0.000
D	2	0.72	0.358	0.37	0.693
M	5	247.47	49.494	50.95	0.000
SD	5	4145.98	829.195	853.63	0.000
Error	95	92.28	0.971		
Total	107	4486.44			

Table-3.3. Analysis of variance (ANOVA) for Elastic modulus.

Source	DF	Adj SS	Adj MS	F-Value	P-Value
Model	12	11048344	920695	385.66	0.000
Linear	12	11048344	920695	385.66	0.000
D	2	2608	1304	0.55	0.581
M	5	613355	122671	51.38	0.000
SD	5	10432381	2086476	873.97	0.000
Error	95	226798	2387		
Total	107	11275142			

Significant terms deviate from the straight line in the center of the normal effects plot or exceed the threshold of the Pareto chart [35]. According to the Pareto chart in Figure-3.2, the terms composite materials (M) and strut diameter (SD) appear significant and exceed the threshold. At the 5% significance level, the Pareto chart shows that composite materials (M) and strut diameter (SD) are the most important factors for compressive strength and elastic modulus.

VOL. 18, NO. 6, MARCH 2023 ISSN 1819-6608
ARPN Journal of Engineering and Applied Sciences

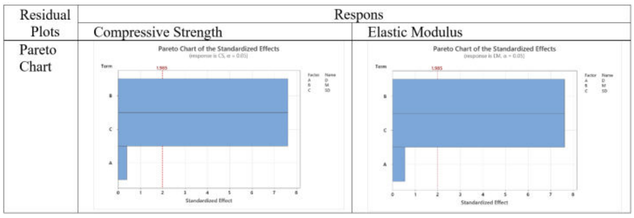

Figure-3.2. Pareto chart of compressive strength and elastic modulus.

Before further statistical analysis, model adequacy checking was undertaken to validate numerous residual assumptions [36]. The adequacy checking regulates three residual assumptions: (i) the residuals' normality assumption; (ii) the residuals' constant variance; and (iii) the residuals' independence. If these assumptions are correct, the generated regression model is primarily valid for the experimental data [37]. Several statistical residual plots, such as the normal probability, versus fit, histogram, and versus order, might be used to verify the three assumptions [33].

The residual plots for compressive strength and elastic modulus of the irregularly shaped bone scaffolds are shown in Figure-3.3 and Figure-3.4. It was discovered by evaluating the normal probability plots that all residual points are spaced around the straight line, indicating that the compressive strength and elastic modulus are normally distributed. It indicates that the model adequacy checking's first criterion was satisfied.

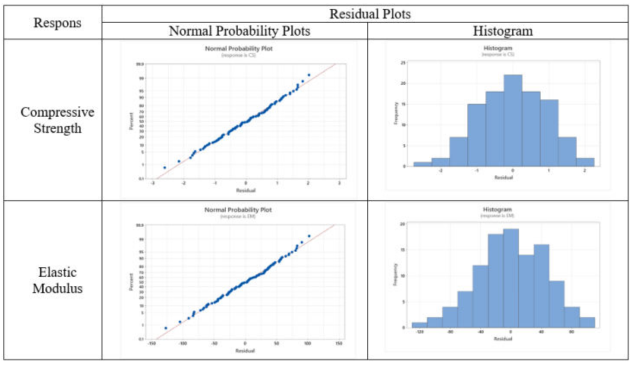

Figure-3.3. Model adequacy residual plots for assessing the normal probability and histogram.

The distribution of the residuals for each observation is shown in a residuals histogram. The virtually symmetrical histogram in the illustration indicates that the errors are normally distributed with a mean of zero. The residual versus fitted value graphs demonstrated that the data points for compressive strength and elastic modulus are randomly distributed with no notable structure. As a result, the residuals' constant variance seems to be acceptable. Moreover, residual versus order plots demonstrated that residual points are fully random, regardless of observation order. It means that the residuals were independent of one another and conformed to their independence to be acceptable.

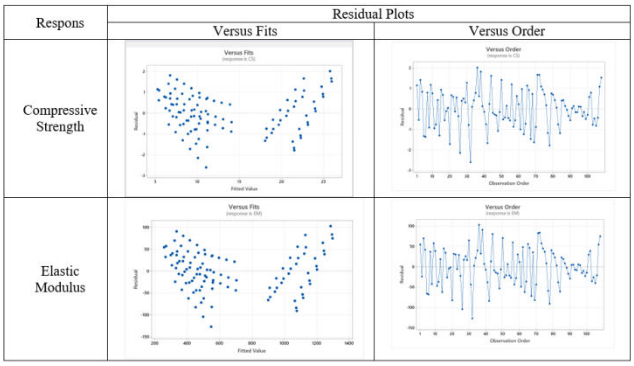

Figure-3.4. Model adequacy residual plots for assessing the versus fits and order.

3.3 Main and Interaction Effects

According to the graphs in Figure-3.5.a, the strut diameter (SD) was the most critical variable in the simulation study. The positive sign of this coefficient means that increasing strut diameter (SD) can increase the compressive strength and elastic modulus of an irregular porous scaffold. Increasing the strut diameter (SD) from 0.55 to 0.6 mm increased the compressive strength by 73.77% and the elastic modulus by 73.83%. A similar trend may be seen in the impact of material composition. The compressive strength and elastic modulus increased by 7.08% and 7.08%, respectively, when the hydroxyapatite composition was raised from 5 to 10%.

The effects of various porosities on the compressive strength and elastic modulus of scaffolds are investigated by evaluating various combinations of strut diameter to produce a variety of porosities. All of the scaffold specimens simulated in this section have a unit cell size of 4 mm. The compressive strength and elastic modulus decrease with increasing porosity, which is explained by the fact that the porous structure reduces material carrying capacity. Numerous studies have documented this common tendency [22, 38, 39], and it has been obliquely argued that densification is supposed to relieve stress concentrations in the matrix by minimizing undesired matrix defects. Naturally, the more porous the structure, the greater the number of defects in the composites [38]. The maximum compressive strength and elastic modulus were obtained using a 0.65 mm strut diameter. It means that the porosity of the irregular structure is 48%. Some researchers recommend the porosity of bone scaffolds be at least 50% [29, 32, 40-42]. Based on these suggestions, an irregular porous scaffold with a strut diameter of between 0.6 and 0.65 mm may be recommended. The elastic modulus of trabecular bone structure may have distinct values in the longitudinal and transverse directions, making it extremely anisotropic [43]. In contrast, the cancellous bone may be essentially isotropic in some areas, such as the proximal section of the bovine humerus [43]. This study found that the variation of loading orientation at all irregular porous scaffolds in this research does little to affect compressive strength and elastic modulus, which makes them more suited for

ARPN Journal of Engineering and Applied Sciences

environments requiring isotropic mechanical characteristics.

The main inorganic component of human bones is hydroxyapatite (HA). It is biocompatible, stable, and easily degraded [44]. HA promotes osteoblast adhesion and growth, as well as the release of extracellular matrix and the formation of chemical interactions with the bones [45,46]. Because it is so similar to bone, HA is used in bone tissue engineering research. Because HA does not cause inflammatory reactions when used in clinical settings, its powders are used as bone fillers or as a coating over metal bone prostheses [47]. According to the findings of this study, HA content is another factor that influences the mechanical properties of irregular porous scaffolds. Figure-7 shows that the compressive strength and elastic modulus of the porous scaffold increase as the HA concentration increases. These findings differ significantly from those of other researchers. Zhang *et al.* [48] discovered that as the HA content of the composite scaffold increased, its compressive strength decreased, while the elastic modulus of the composite scaffold was unaffected. Wang *et al.* [49] discovered that adding more HA reduced its mechanical strength. While some studies found that increasing the HA content had no effect on the mechanical properties of the bone scaffold, others discovered the opposite. Our findings agreed with those of Wu *et al.* [18], who discovered that adding HA increased the elastic modulus significantly. According to Li *et al.*, the elastic modulus and compressive strength of the created scaffold are also influenced by the size of the macrospore and the presence of HA nanoparticles. They observe an increase in the elastic modulus of the porous scaffold as the number of HA increases [50]. Increased HA concentration resulted in improved mechanical properties. Hassanajili *et al.* [19] also concluded that higher HA content improved bone scaffold compression strength and elastic modulus.

The interaction-effects plots are shown in Figure-3.5.b. The non-parallel lines in this diagram represent the interaction of the three variables. Figure-7b shows that the interaction of the loading direction (D) and material composition (M) has no effect on the compressive strength and elastic modulus responses. Similarly, when loading direction (D) and strut diameter interact (SD). However, the interaction between the material composition (M) and the strut diameter (SD) forms a non-parallel line, indicating that the interaction influences the response, even though it is minor. This means that, when compared to other variables, strut diameter (SD) has the most significant effect.

3.4 Response Optimizer

The optimum condition of controllable variables or components that would result in the required qualities of an irregular porous scaffold can be established using a response optimizer method. The objectives were for maximum responses (compressive strength and elastic modulus). Figure-3.6. depicts the optimization plot for the desired responses. The composite desirability (D) [33,51] is another statistical parameter that can be used to validate the accuracy of the optimization plot. The closer D is to 1.00, the more reliable and precise the statistical analysis factors and response optimization [52]. The compressive strength and elastic modulus of response optimization of composite desirability are 0.9159 and 0.0917, respectively. As a result, the optimization plot's optimal conditions were very reliable and strictly adhered to the established regression models. These desired results were obtained using the Z loading direction, 30% hydroxyapatite composition, and 0.65 mm strut diameter, according to the simulation. The maximum compressive strength and elastic modulus were calculated to be 25.93 and 1295.24 MPa, respectively.

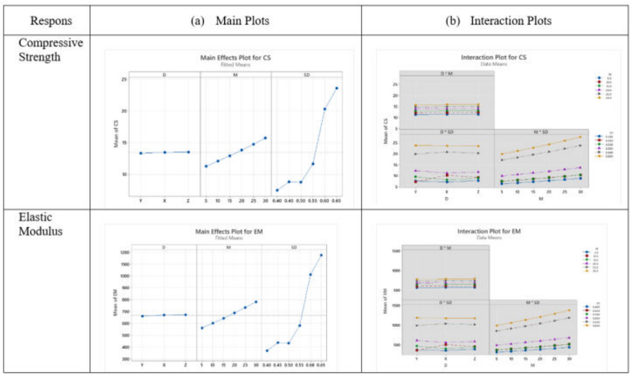

Figure-3.5. Main and interaction plots.

These findings indicate that the compressive strength and elastic modulus of the bone scaffold are lower than cortical bone but within the range of trabecular bone. Cortical bone has compressive strength and elastic modulus of 113-225 MPa and 10-22 Gpa, respectively, while trabecular has 4-25 MPa and 0.7-30 Gpa[18].

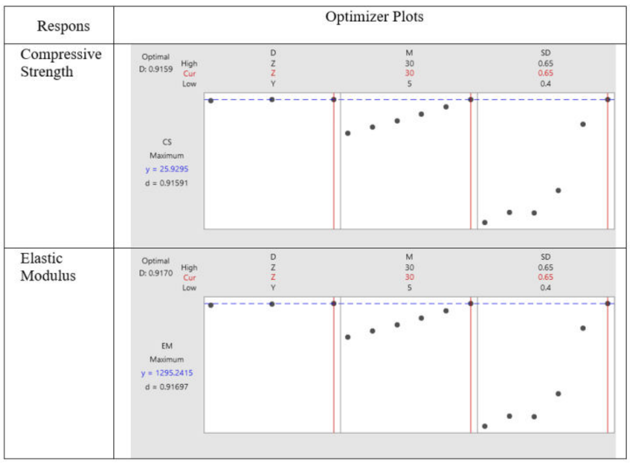

Figure-3.6. Response optimization plot.

4. CONCLUSIONS

Finite element analysis can be used to predict the mechanical properties of irregular porous scaffolds before they are built. Using finite element analysis, this study investigated the morphological and mechanical properties of six distinct irregular porous structure designs with varying material compositions, strut diameters, and loading orientations. A full factorial design of experiments was used to determine the optimal mechanical properties of an irregularly shaped scaffold design. Our findings show that composite materials and strut diameter are important factors in compressive strength and elastic modulus. Nonetheless, in this simulation study, the strut diameter was the most critical variable. The results show a linear relationship between composite materials and the mechanical properties of the irregular porous scaffold. This study also found that variation of loading direction at all irregular porous scaffolds in this research does little to affect compressive strength and elastic modulus, which makes them more suited for environments requiring isotropic mechanical characteristics. The optimization method showed that the desired results are obtained with the Z loading direction, 30% hydroxyapatite composition, and 0.65 mm strut diameter. The maximum compressive strengthened elastic modulus was calculated to be 25.93 MPa and 1295.24 MPa, respectively. These results suggest that the bone scaffold's elastic modulus and compressive strength are comparable to the trabecular bone but less than cortical bone. Additional experimental mechanical testing, in vitro and in vivo, will be required to determine the clinical applicability of bone scaffolds with an irregular porous design.

ACKNOWLEDGMENTS

This work was supported by the Deputy for Strengthening Research and Development, the Ministry of Research and Technology, Higher Education, the Republic of Indonesia under Ph.D. research grants of number: 088/ES/PG.02.00.PT/2022; 345-35/UN7.6.1/PP/2022.

Conflict of interest

The authors declare no conflict of interest.

REFERENCES

[1] T. Sosakul, J. Suwanprateeb, and B. Rungroungdouyboon. 2021. Current applications of porous polyethylene in tissue regeneration and future use in alveolar bone defect. Asia-Pacific J. Sci. Technol. 26(04): 1-10.

[2] H. Chen, Q. Han, C. Wang, Y. Liu, B. Chen and J. Wang. 2020. Porous Scaffold Design for Additive Manufacturing in Orthopedics: A Review. Front. Bioeng. Biotechnol., 8(June): 1-20, doi: 10.3389/fbioe.2020.00609.

[3] S. J. Hollister, R. A. Levy, T. M. Chu, J. W. Halloran, and S. E. Feinberg. 2000. An image-based approach for designing and manufacturing craniofacial scaffolds. Int. J. Oral Maxillofac. Surg., 29(1): 67-71, doi: 10.1034/j.1399-0020.2000.290115.x.

[4] X. Wang *et al*. 2016. Topological design and additive manufacturing of porous metals for bone scaffolds and orthopaedic implants: A review. Biomaterials, 83: 127-141, doi: 10.1016/j.biomaterials.2016.01.012.

[5] H. Chen *et al*. 2021. Design and properties of biomimetic irregular scaffolds for bone tissue engineering. Comput. Biol. Med., 130(November 2020), doi: 10.1016/j.compbiomed.2021.104241.

[6] A. Nazir, K. M. Abate, A. Kumar and J. Y. Jeng. 2019. A state-of-the-art review on types, design, optimization, and additive manufacturing of cellular structures. Int. J. Adv. Manuf. Technol., 104(9-12): 3489-3510, doi: 10.1007/s00170-019-04085-3.

[7] L. J. Gibson. 2005. Biomechanics of cellular solids. J. Biomech., 38(3): 377-399, doi: 10.1016/j.jbiomech.2004.09.027.

[8] A. Syahrom, M. R. Abdul Kadir, J. Abdullah and A. Öchsner. 2013. Permeability studies of artificial and natural cancellous bone structures. Med. Eng. Phys., 35(6): 792-799, doi: 10.1016/j.medengphy.2012.08.011.

[9] A. Cheng, A. Humayun, D. J. Cohen, B. D. Boyan and Z. Schwartz. 2014. Additively manufactured 3D porous Ti-6Al-4V constructs mimic trabecular bone structure and regulate osteoblast proliferation, differentiation and local factor production in a porosity and surface roughness dependent manner. Biofabrication, 6(4), doi: 10.1088/1758-5082/6/4/045007.

[10] H. Liang *et al*. 2019. Trabecular-like Ti-6Al-4V scaffolds for orthopedic: fabrication by selective laser melting and in vitro biocompatibility. J. Mater. Sci. Technol., 35(7): 1284-1297, doi: 10.1016/j.jmst.2019.01.012.

[11] J. Deering, K. I. Dowling, L. A. DiCecco, G. D. McLean, B. Yu, and K. Grandfield. 2021. Selective Voronoi tessellation as a method to design anisotropic and biomimetic implants. J. Mech. Behav. Biomed. Mater., 116(June 2020), doi: 10.1016/j.jmbbm.2021.104361.

[12] H. Zhao *et al*. 2021. Design and mechanical properties verification of gradient voronoi scaffold for bone tissue engineering. Micromachines, 12(6): 1-23, doi: 10.3390/mi12060664.

[13] M. Fantini, M. Curto and F. De Crescenzio. 2016. A method to design biomimetic scaffolds for bone tissue engineering based on Voronoi lattices. Virtual Phys. Prototyp., 11(2): 77-90, doi: 10.1080/17452759.2016.1172301.

[14] Y. Du *et al*. 2020. Design and statistical analysis of irregular porous scaffolds for orthopedic reconstruction based on voronoi tessellation and fabricated via selective laser melting (SLM). Mater. Chem. Phys., 239(August 2019): 121968, doi: 10.1016/j.matchemphys.2019.121968.

[15] M. Alkhader and M. Vural. 2008. Mechanical response of cellular solids: Role of cellular topology and microstructural irregularity. Int. J. Eng. Sci., 46(10): 1035-1051, doi: 10.1016/j.ijengsci.2008.03.012.

[16] S. A. Sampath, S. Lewis, M. Fosco and D. Tigani. 2015. Trabecular orientation in the human femur and tibia and the relationship with lower-limb alignment for patients with osteoarthritis of the knee. J. Biomech., 48(6): 1214-1218, doi: 10.1016/j.jbiomech.2015.01.028.

[17] K. Chavalitpanya and S. Phattanarudee. 2013. Poly(lactic acid)/polycaprolactone blends compatibilized with block copolymer. Energy Procedia, 34: 542-548, doi: 10.1016/j.egypro.2013.06.783.

[18] D. Wu, A. Spanou, A. Diez-Escudero and C. Persson. 2020. 3D-printed PLA/HA composite structures as synthetic trabecular bone: A feasibility study using fused deposition modelling. J. Mech. Behav. Biomed. Mater., 103(August 2019): 103608, doi: 10.1016/j.jmbbm.2019.103608.

[19] S. Hassanajili, A. Karami-Pour, A. Oryan and T. Talaei-Khozani. 2019. Preparation and characterization of PLA/PCL/HA composite scaffolds using indirect 3D printing for bone tissue engineering. Mater. Sci. Eng. C, 104(July): 109960, doi: 10.1016/j.msec.2019.109960.

[20] I. Gendviliene *et al*. 2020. Assessment of the morphology and dimensional accuracy of 3D printed PLA and PLA/HAp scaffolds. J. Mech. Behav. Biomed. Mater., vol. 104, doi: 10.1016/j.jmbbm.2020.103616.

[21] E. Mystiridou, A. C. Patsidis and N. Bouropoulos. 02021. Development and characterization of 3D printed multifunctional bioscaffolds based on PLA/PCL/HAp/BaTiO3 composites. Appl. Sci., 11(9), doi: 10.3390/app11094253.

[22] B. Zhang, L. Guo, H. Chen, Y. Ventikos, R. J. Narayan and J. Huang. 2020. Finite element evaluations of the mechanical properties of polycaprolactone/hydroxyapatite scaffolds by direct ink writing: Effects of pore geometry. J. Mech. Behav. Biomed. Mater., 104(January, 2020), doi: 10.1016/j.jmbbm.2020.103665.

[23] H. Kaul, B. K. Hall, C. Newby and Y. Ventikos. 2015. Synergistic activity of polarised osteoblasts inside condensations cause their differentiation. Sci. Rep., 5: 1-19, doi: 10.1038/srep11838.

[24] A. D. Bagde *et al*. 2019. Geometric Modeling and Finite Element Simulation for Architecture Design of 3D Printed Bio-ceramic Scaffold Used in Bone Tissue Engineering. J. Indian Inst. Sci., 99(3): 361-374, doi: 10.1007/s41745-019-00120-0.

[25] S. Farah, D. G. Anderson and R. Langer. 2016. Physical and mechanical properties of PLA, and their functions in widespread applications - A comprehensive review. Adv. Drug Deliv. Rev., 107: 367-392, doi: 10.1016/j.addr.2016.06.012.

[26] J. K. Bagwan, B. B. Ahuja, A. V. Mulay and K. J. Jawale. 2022. Geometrical analysis of extrusion based (Additively Manufactured) 3D designed scaffold for bone tissue engineering: A finite element approach. Mater. Today Proc., 50: 1465-1471, doi: 10.1016/j.matpr.2021.09.049.

[27] Z. Yuan, F. Li, P. Zhang, B. Chen and F. Xue. 2014. Mechanical properties study of particles reinforced aluminum matrix composites by micro-indentation experiments. Chinese J. Aeronaut., 27(2): 397-406, doi: 10.1016/j.cja.2014.02.010.

[28] G. A. P. Renders, L. Mulder, L. J. van Ruijven, and T. M. G. J. van Eijden. 2007. Porosity of human mandibular condylar bone. J. Anat., 210(3): 239-248, doi: 10.1111/j.1469-7580.2007.00693.x.

[29] S. Arabnejad, R. Burnett Johnston, J. A. Pura, B. Singh, M. Tanzer and D. Pasini. 2016. High-strength porous biomaterials for bone replacement: A strategy to assess the interplay between cell morphology, mechanical properties, bone ingrowth and manufacturing constraints. Acta Biomater., 30: 345-356, doi: 10.1016/j.actbio.2015.10.048.

[30] M. S. Tang, A. Z. Abdul Kadir and N. H. A. Ngadiman. 2020. Simulation analysis of different bone scaffold porous structures for fused deposition modelling fabrication process. in 5th International Conference on Mechanical Engineering Research 2019, ICMER 2019, 788(1), doi: 10.1088/1757-899X/788/1/012023.

[31] ASTM_D695_Compression.pdf. p. 48.

[32] L. Mullen, R. C. Stamp, W. K. Brooks, E. Jones and C. J. Sutcliffe. 2009. Selective laser melting: A regular unit cell approach for the manufacture of porous, titanium, bone in-growth constructs, suitable for orthopedic applications. J. Biomed. Mater. Res. - Part B Appl. Biomater., 89(2): 325-334, doi: 10.1002/jbm.b.31219.

[33] P. Ter Teo *et al*. 2021. Application of general full factorial statistical experimental design's approach for the development of sustainable clay-based ceramics incorporated with malaysia's electric arc furnace steel slag waste. Crystals, 11(4): 50-52, doi: 10.3390/cryst11040442.

[34] O. Prakash, M. Talat, S. H. Hasan and R. K. Pandey. 2008. Factorial design for the optimization of enzymatic detection of cadmium in aqueous solution using immobilized urease from vegetable waste. Bioresour. Technol., 99(16): 7565-7572, doi: 10.1016/j.biortech.2008.02.008.

[35] A. Mazen, B. McClanahan and J. M. Weaver. 2022. Factors affecting ultimate tensile strength and impact toughness of 3D printed parts using fractional factorial design. Int. J. Adv. Manuf. Technol., 119(3-4): 2639-2651, doi: 10.1007/s00170-021-08433-0.

[36] S. H. A. Rahman, N. N. Zulkarnain and N. Shafiq. 2021. Experimental study and design of experiment using statistical analysis for the development of geopolymer matrix for oil-well cementing for enhancing the integrity. Crystals, 11(2), doi: 10.3390/cryst11020139.

[37] S. Saadat and A. Karimi-Jashni. 2011. Optimization of Pb(II) adsorption onto modified walnut shells using factorial design and simplex methodologies. Chem. Eng. J., 173(3): 743-749, doi: 10.1016/j.cej.2011.08.042.

[38] X. L. Liao, W. F. Xu, Y. L. Wang, B. Jia and G. Y. Zhou. 2009. Effect of porous structure on mechanical properties of C/PLA/nano-HA composites scaffold. Trans. Nonferrous Met. Soc. China (English Ed., 19(SUPPL. 3): s748-s751, doi: 10.1016/S1003-6326(10)60144-6.

[39] M. Khodaei, K. Amini, and A. Valanezhad. 2020. Fabrication and Characterization of Poly Lactic Acid Scaffolds by Fused Deposition Modeling for Bone Tissue Engineering. J. Wuhan Univ. Technol. Mater. Sci. Ed., 35(1): 248-251, doi: 10.1007/s11595-020-2250-4.

[40] S. J. Hollister. 2006. Porous scaffold design for tissue engineering (vol 4, pg 518, 2005). Nat. Mater., 5(7): 590.

[41] H. A. Zaharin *et al*. 2018. Effect of unit cell type and pore size on porosity and mechanical behavior of additively manufactured Ti6Al4V scaffolds. Materials (Basel)., 11(12), doi: 10.3390/ma11122402.

[42] Z. Cai, Z. Liu, X. Hu, H. Kuang and J. Zhai. 2019. The effect of porosity on the mechanical properties of 3D-printed triply periodic minimal surface (TPMS) bioscaffold. Bio-Design Manuf., 2(4): 242-255, doi: 10.1007/s42242-019-00054-7.

[43] J. L. Williams and J. L. Lewis. 1982. Properties and an anisotropic model of cancellous bone from the proximal tibial epiphysis. J. Biomech. Eng., 104(1): 50-56, doi: 10.1115/1.3138303.

[44] M. Askari, M. Afzali Naniz, M. Kouhi, A. Saberi, A. Zolfagharian and M. Bodaghi. 2021. Recent progress in extrusion 3D bioprinting of hydrogel biomaterials for tissue regeneration: A comprehensive review with focus on advanced fabrication techniques. Biomater. Sci., 9(3): 535-573, doi: 10.1039/d0bm00973c.

[45] A. Alinda Shaly, G. Hannah Priya and J. Mary Linet. 2021. An exploration on the configurational and mechanical aspects of hydrothermally procured MgO/HA bioceramic nanocomposite. Phys. B Condens. Matter, 617(January): 413131, doi: 10.1016/j.physb.2021.413131.

[46] W. Wang *et al*. 2021. 3D printing of PLA/n-HA composite scaffolds with customized mechanical properties and biological functions for bone tissue engineering. Compos. Part B Eng., vol. 224, doi: 10.1016/j.compositesb.2021.109192.

[47] F. Baino, G. Novajra and C. Vitale-Brovarone. 2015. Bioceramics and scaffolds: A winning combination

for tissue engineering. Front. Bioeng. Biotechnol., 3(December): 1-17, doi: 10.3389/fbioe.2015.00202.

[48] B. Zhang *et al*. 2021. 3D printed bone tissue regenerative PLA/HA scaffolds with comprehensive performance optimizations. Mater. Des., 201: 109490, doi: 10.1016/j.matdes.2021.109490.

[49] W. Wang *et al*. 2021. 3D printing of PLA/n-HA composite scaffolds with customized mechanical properties and biological functions for bone tissue engineering. Compos. Part B Eng., 224(July): 109192, doi: 10.1016/j.compositesb.2021.109192.

[50] X. Li *et al*. 2021. Experimental measurement and simulation of mechanical strength and biological behavior of porous bony scaffold coated with alginate-hydroxyapatite for femoral applications. Compos. Sci. Technol., 214(May), doi: 10.1016/j.compscitech.2021.108973.

[51] M. Ciopec *et al*. 2012. Adsorption studies of Cr(III) ions from aqueous solutions by DEHPA impregnated onto Amberlite XAD7 - Factorial design analysis. Chem. Eng. Res. Des., 90(10): 1660-1670, doi: 10.1016/j.cherd.2012.01.016.

[52] B. Peng Chang, H. Md Akil, R. Bt Nasir and A. Khan. 2015. Optimization on wear performance of UHMWPE composites using response surface methodology. Tribol. Int., 88: 252-262, doi: 10.1016/j.triboint.2015.03.028.